Transient Analysis of Thermal Bending and Vibration of Steam Turbine Rotor

Nonso Omenife[1,2], Dawood Desai[1], Regan Dunne[1]

[1]*Department of Mechanical and Mechatronics Engineering. Tshwane University of Technology, Pretoria South Africa*
[2]*Department of Mechanical/ Production Engineering, Nnamdi Azikiwe University. Awka, Anambra state Nigeria*

Abstract

Rotor-bearing systems often exhibit nonlinear behavior due to hydrodynamic effects and external forces. Finite element methods based on linear analysis are commonly used for rotor dynamic analyses, where nonlinear bearing/damping forces are linearized into equivalent stiffness and damping coefficients. However, this method may not accurately describe strongly nonlinear systems. Engineers use transient analysis and nonlinear models to improve rotor behavior analysis. This study investigates the effects of transient-thermal bending and vibration on a high-pressure steam turbine rotor using the finite element method. A scaled rotor-shaft was used to study thermal bending and vibrations caused by steam heat. The design of the shaft was based on an existing power station high-pressure turbine rotor. Numerical modal analyses were performed using ANSYS software to obtain a partial level of integrity between the numerical model and the analytical model. Natural frequencies were compared between the experimental, numerical, and analytical results, which showed good correlations.

Keywords: *rotor, transient analysis, vibrations, analytical analysis, numerical analysis*

1. Introduction

Rotating machinery such as turbines and compressors, is critical equipment in power generation and petrochemical plants. Thermal loading owing to high steam temperatures on steam turbine rotor shafts can cause the rotor to bend, leading to steam turbine rotor vibrations and subsequently, plant shutdown, as significant heat exchange occurs between the steam and turbine rotors during the start-up process. Even more intensive heat exchange occurs during the condensation phase in the cold start-up mode, which leads to further thermal stresses and lifetime reduction [1] according to Sátor et al. Therefore, the accuracy of lifetime prediction is strongly affected and dependent on the accuracy of the transient thermal state, allowing engineers to design more efficient and reliable systems.

Some relevant studies under transient analysis are covered in the references [2-9]. In this study, transient analysis of the thermal bending and vibration of steam turbine rotors was explored using finite element analysis (FEA) simulation with analytical validation. The most common causes of rotor vibration include weight imbalance, bearing misalignment, resonance, bearing malfunction, and unbalanced electromagnetic forces in the generator, because excessive rotor vibration can cause rubbing and impact damage to components such as turbine seals. High-speed turbines are a major source for power production utilizing high pressure and temperature fluid flow. By considering the transient behavior of thermal bending in steam turbine rotor-shafts, engineers can optimize the design and operation of these critical components, leading to improved efficiency and reliability of power generation systems. The design of the rotor itself can also play a role in its response to thermal loads. For example, the use of cooling channels within the rotor can help to mitigate temperature gradients and reduce thermal stresses, as noted by Chatterton et. Al. [10].

Corresponding author: Nonso Omenife *(omenifeu@yahoo.com)*
Received: *19 June 2023*; Revised: *14 July 2023*; Accepted: *17 July 2023*; Published: 20 *July 2023*

This study aims to gain insight into finite element analysis and analytical methods by comparing the output of a computer model with analytical data. The study uses Finite Element Analysis (FEA) to estimate the effects of transient thermal and vibration spectra on a turbine rotor-shaft, with the goal of making recommendations for the design and operation of the rotor. To accomplish this, a typical turbine rotor-shaft was modeled using ANSYS Workbench to perform a transient analysis of thermal bending. Transient thermal stresses and deformations are investigated, and the results provide insights into the structural integrity and fatigue life of the rotor under varying thermal conditions. By investigating the transient behavior of rotors under varying thermal conditions, we concluded that the transient analysis of thermal bending and vibration of steam turbine rotors is an area of critical research and engineering interest. Accurate prediction and understanding of the rotor's transient behavior contribute to optimizing turbine design, enhancing performance, and ensuring safe and reliable operation. Through the incorporation of advanced computational techniques and consideration of various operating parameters, researchers and engineers can continue to advance our knowledge and develop effective strategies to mitigate challenges associated with thermal bending and vibration in steam turbine rotors. Some relevant studies pertaining to rotor's transient analysis behavior with turbine design are cited in the references [11-13].

2. Methodology

The simulation was achieved based on transient thermal bending and rotor vibration using the commercial software ANSYS**.** We implemented Finite Element Method (FEM) software to research the transient thermal bending and rotor vibration. We performed variations for temperature and rotational speed of the rotor shaft. Numerical techniques in the form of FEA simulation and analytical techniques for validation were used in this study. This was achieved by developing a numerical model for the transient analysis of rotor vibration and thermal bending of the HP turbine.

Modal analysis techniques, such as the finite element method and analytical approaches, are employed to determine the system's dynamic characteristics. Coupled analysis was employed, whereby transient-thermal analysis was combined with transient-structural analysis to account for the interaction between temperature distribution and resulting rotor deformations, which is achieved through a coupled analysis, where the transient-thermal results were used as input for the transient-structural analysis. The process is typically iterative, with information being exchanged between the thermal and structural solvers until convergence is achieved.

2.1. Mesh convergence study

In this study, a variety of mesh sizes were used in the simulation to check mesh convergence. Each mesh density was plotted against the rotor surface temperature results, and it reached a critical point when the solutions approach the optimum mesh density. However, Figure 1 below shows the rotor-shaft mesh used in ANSYS simulations. A detailed drawing of the rotor-shaft under study is shown in the appendix A.

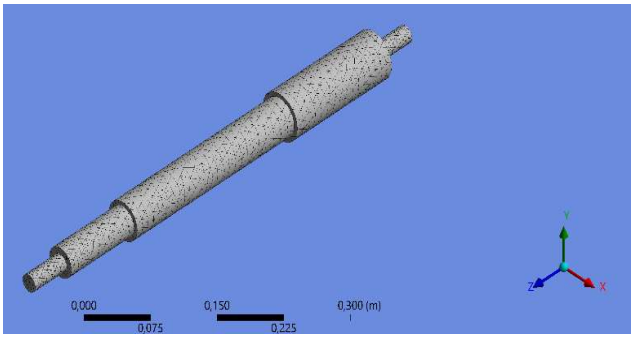

Figure 1. Structured mesh of the rotor-shaft

The rotor-shaft simulation model meshed with structural mesh elements, to be specific tetrahedral elements, also known as solid/brick elements. These mesh elements were chosen due to their solution accuracy, better mesh convergence, flexibility, increased adaptability, improved simulation speed, and reduced mesh generation effort over hexahedral mesh elements.

In finite element analysis (FEA) convergence means arriving at the true solution of the partial differential equations (PDEs) as the geometry, or spatial domain, is meshed more finely. A mesh convergence plot is shown in Figure 2. The mesh size for a given solution is found where it does not change further, and all subsequent simulations are based on this.

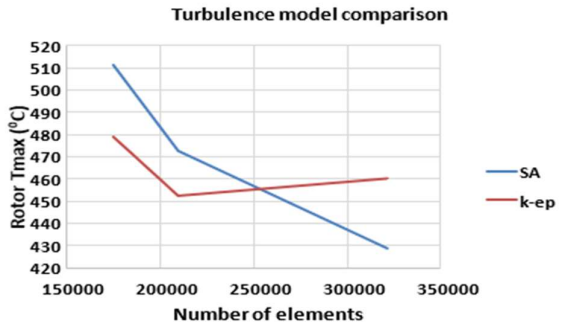

Figure 2. Mesh convergence illustration (source: k-epsilon turbulence model).

To ensure good convergence, 2000 iterations were used, and the convergence was monitored for a change in the solution during the solution iteration. The rotor-shaft maximum temperature shows no changes in any of the convergence monitoring values, thus, it shows the simulation had reached convergence. The turning point in the plot for a mesh with 209 727 elements determined the choice of k-epsilon turbulence model, so the simulations were conducted using this mesh. Figure 3 illustrates the k-epsilon turbulence model convergence residuals.

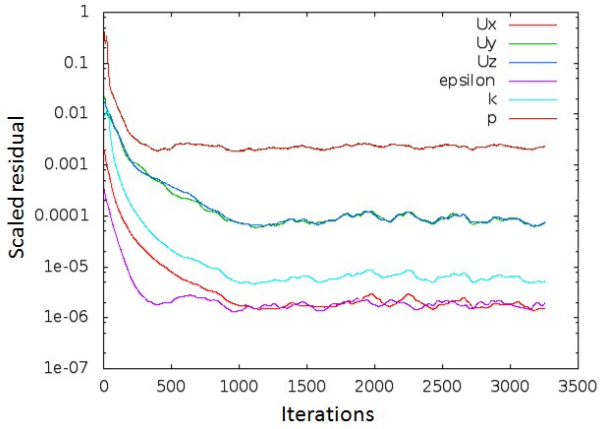

Figure 3. Illustration of k-epsilon turbulence model convergence residuals.

Tetrahedral elements are used because they fit arbitrary shaped geometries very well with their simple computations. Different meshes are developed with different body, face, edge sizing controlled in ANSYS workbench. Moreover, the results of an FEA model must be independent of mesh size, as the convergence study ensures the FEA model captures the system's behavior, while reducing solve time.

2.2. Boundary conditions

The rotor-shaft model rotates with respect to the global cartesian X-axis. With respect to the X-axis, we apply angular velocity and use a degree of freedoms along UX, UZ, ROTY, ROTZ at bearing ends. In areas where bearing supports will be used, the operator inputs different angular velocities and measures the corresponding accelerations at both the drive end and non-drive end. Fixed supports will be applied on the rotor shaft, a rotational speed of 3 000 revolutions per minute was applied to the shaft of the rotor, and the picture below demonstrates the boundary conditions.

Figure 4. Boundary Conditions

3. Numerical modal analysis setup and results

ANSYS Mechanical workbench 2021 was used for the numerical simulation of natural frequencies. Free-free boundary conditions were used in the simulation, and structural steel was the material of choice. In this analysis, no rotation was activated, meaning that centrifugal forces were not present on the modal analysis simulation. Hence, the Coriolis effect was not considered, and no damping setting was activated for the analysis. The mode shape results of mode eight are shown in Figure 5, and Table 1 shows the natural frequency results. The appendix section under appendix B contains the mode shapes for the rest of the modes.

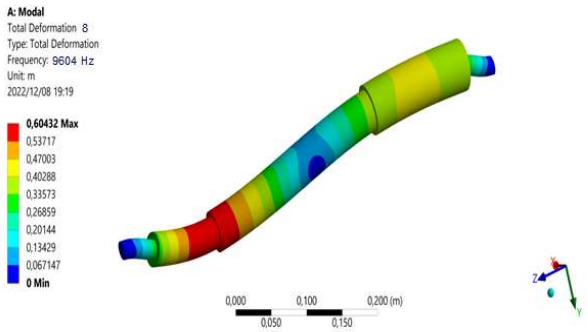

Figure 5. Mode shape eight results.

Table 1. Simulation results of Eigen frequencies.

Eigen frequency (Hz)	Mode
295	01
762	02
1790	03
3169	04
4439	05
5470	06
6928	07
9604	08

3.1. Analytical modal analysis and solutions

Analytical solutions are also available for stationary and transient cases of cylinders and collars (extended surfaces) under the conditions of radiation and convection board, if the thermal conductivity is constant and isotropic by Smith et al. In cases where the conductivity is anisotropic and a strong function of temperature, or the material is not homogeneous, an exact solution does not exist. The tested shaft in this work can be considered as a horizontal slender cylindrical beam with uniformly distributed mass, subjected to forces applied perpendicularly to the axis of the shaft. The Bernoulli-Euler-Timoshenko beam theory supposed that any plane cross-section of slender beams remains plane and normal to the longitudinal axis during small bending. This assumption simplifies the solution of the equation of motion to extract the natural frequencies and mode shapes of the rotor-shaft under study. Depending on the theory mentioned above and applying free-free boundary conditions in the modal solution of the equation of motion, provides the natural frequencies equation below.

$$\mathfrak{f}_i = \frac{\lambda_1^2}{2\pi L^2}\sqrt{\frac{EI_z}{m}}, H_z, i = 1,2,3 \ldots . n \tag{1}$$

where E, I_z and m are, modulus of elasticity, area moment of inertia of cross section about z-axis through the centroid, and mass per unit length, respectively. However, for the analytical extraction of mode shapes, according to the Bernoulli-Euler-Timoshenko beam theory mentioned above, the solution of the equation of motion below extracts the mode shapes under study. A structural steel solid shaft body of 600 mm in length and 35 mm in diameter is taken as a case study. Material properties of the shaft are mass density is 7850 kg/m^3, modulus of elasticity is 200 MPa, and Poisson's ratio is 0.3.

$$\widetilde{Yi}\left(\frac{\lambda ix}{L}\right) = Cosh\frac{\lambda ix}{L} + Cos\frac{\lambda ix}{L} - \alpha i\left(Sinh\frac{\lambda ix}{L} + Sin\frac{\lambda ix}{L}\right) \tag{2}$$

where x and $\widetilde{Yi}$ are axial coordinate and lateral displacement, respectively. Natural frequencies, and Mode shapes will be examined by comparing the results of the dynamic analytical, and numerical simulation. However, the rotor dynamic analytical solution is used for the validation of the rotor-shaft model built in this study, and Table 2 shows the analytical eigenvalues results extracted using equation one above.

Table 2. The values of the dynamic analytical results.

Analytical Eigenvalues results (Hz)	Mode
273	01
754	02
1728	03
2991	04
4128	05
5194	06
6935	07
9302	08

3.2. Rotor vibration

Turbomachinery requires a higher level of vibration analysis than general purpose machinery. This includes identifying natural frequencies or modes of a system to determine if a potential resonance occurs. The complexity of turbomachinery requires this higher level of vibration analysis, which includes understanding the importance of transient data. A rotor may tend to vibrate in any direction, and the vibration falls under any one of the following types: Lateral rotor vibration, Torsional rotor vibration and Axial rotor vibration. This work is focused only on lateral rotor vibrations, as the natural frequencies of lateral vibration are influenced by rotating speed. The rotating machines can become unstable because of lateral vibration. Hence, the overwhelming number of rotor dynamic analysis and designs are mostly related with lateral vibrations, which can cause dynamic bending to the shaft in two mutually perpendicular lateral planes. Moreover, the problem of vibration generally originated when rotors in the turbines bend. This bending often occurs during some of the turbine's operational evolutions, leading to vibration or even system failure

down the line. However, the resulting vibration is not the problem itself, but a symptom of system-wide flaws. In fact, rotor bending is one of the most serious problems that power plants face, as they can limit generation and cause the plant to spend more money and time on operation and maintenance costs. These excessive vibrations associated with the critical speed may lead to permanent deformation of the shaft. Furthermore, it can also lead to large shaft deflections at the critical speed, including large bearing reactions and may be subjected to bearing failure.

4. Results and discussions

According to the natural frequency comparison indicated in Table 3, it was found that the maximum percentage difference was 7%, and the minimum percentage difference was 0.02%. An excellent correlation can be observed between experimental results and numerical results, between analytical results and experimental results, and between numerical results and analytical results as well.

Table 3. Natural Frequency comparison table.

Mode	Numerical Modal Analysis Results (Hz)	Analytical Modal Analysis Results (Hz)	Experimental Modal Analysis Results (Hz)
01	295	273	281
02	762	754	758
03	1789	1728	1776
04	3160	2991	3056
05	4429	4128	4096
06	5373	5194	5264
07	6911	6935	6928
08	9604	9302	9264

Figure 6 shows a good reflection on the statement mentioned regarding excellent correlation and the maximum and minimum percentage differences which were found to be slightly closer to each other.

4.1. Transient thermal analysis and results

Below are the transient thermal analysis results showing temperature changes with respect to time and heat flux in the system. Transient-thermal analysis was linked to transient-structural analysis to determine the transient-structural deformation caused by temperature distribution and instantaneous thermal stresses induced under transient conditions. The transient analysis was run for a period of 30000 seconds. It was found that the temperature distribution does not change anymore at 30000 seconds, hence; the problem has reached steady-state conditions that are governed by Fourier's law. For example, in Figure 7, it is evident that the heat flux profile stabilizes at 30000 seconds.

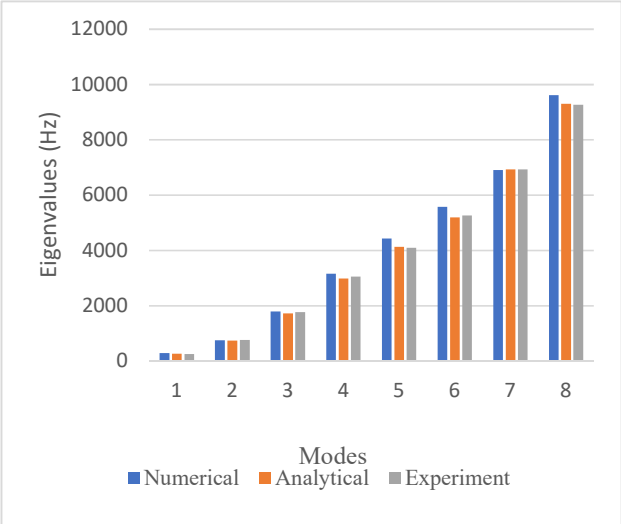

Figure 6. Eigenvalues comparison graph.

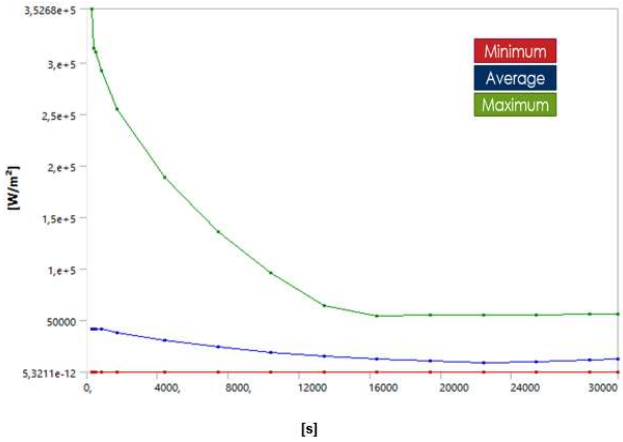

Figure 7. Heat flux profile stabilizes according to Fourier's law.

However, transient-thermal analysis was linked to transient-structural analysis to determine the transient-structural deformation caused by temperature distribution and instantaneous thermal stresses induced under transient conditions. Figures 8 to 12 below show the simulation results in Ansys workbench.

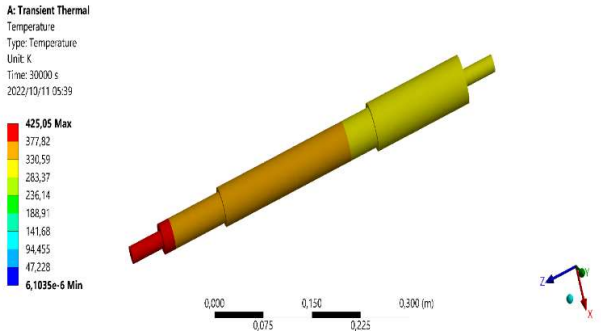

Figure 8. Temperature distribution result in Ansys APDL.

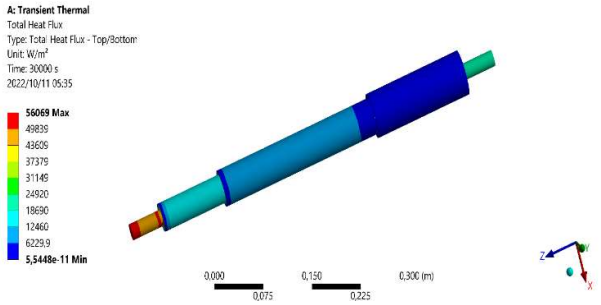

Figure 9. Heat flux result in Ansys APDL.

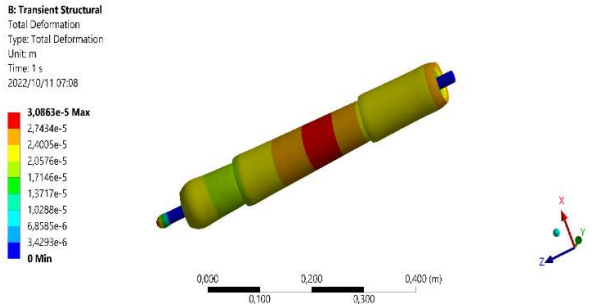

Figure 10. Total transient-thermal to transient-structural deformation result.

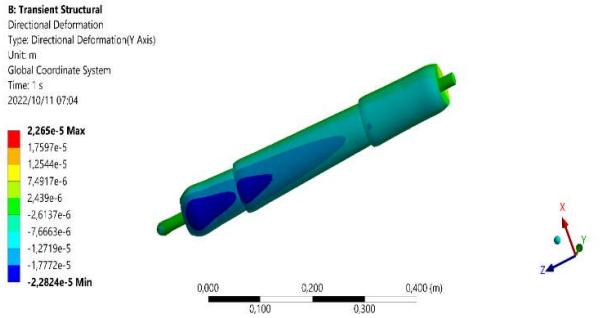

Figure 11. Transient-thermal to transient-structural directional deformation result.

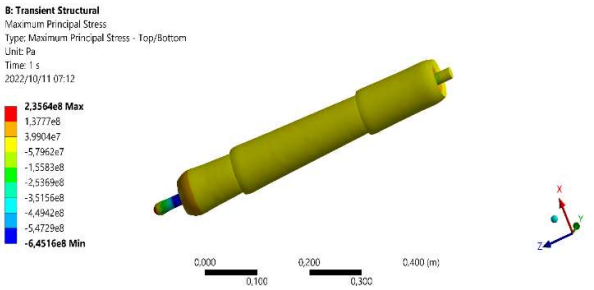

Figure 12. Transient-thermal to transient-structural stress result.

4.2. Analytical solution of thermal moments

When seeking the exact steady solution, we can set the unsteady term of heat conduction Equation 3 on the (right-hand side) to zero. Therefore, the differential equation which governs the steady conduction of heat across a two-dimensional solid (or fluid) in cylindrical coordinates, considering there is no angular variation, with z and r are the only spatial coordinates is:

$$\frac{1}{r}\frac{\partial}{\partial r}\left(r\frac{\partial T}{\partial r}\right)+\frac{\partial^2 T}{\partial z^2}+\frac{W_i}{K}=0 \tag{3}$$

where the body is assumed to be homogeneous, K is the material conductivity and W_i is the constant and uniformly distributed internal heat generation. To make the boundary conditions homogeneous, θ is defined as the spatial temperature distribution referred to the known ambient temperature T_∞. And only half of the rotor length is considered since the problem is symmetrical in the axial position z about z=L. In other words, the origin is replaced in the center of the rotor model and imposed an adiabatic condition at z=0. However, the expressions for T (r, z) from the analytical thermal analysis equation 4 below may as well be inserted into a palmar calculator that has "math" solvers. Hence, evaluating the integration of θ_1 in the numerator and introducing the result the unknown values of C_n expansion coefficient is expressed as:

$$C_n = \frac{\left(\frac{W_i a^2}{2h_\infty}\frac{J_1(\alpha_n a)}{\alpha_n}\right)-\left(\frac{W_i a^2}{2k\alpha_n^2}\right)\left(J_0(\alpha_n a)-\frac{2J_1(\alpha_n a)}{(\alpha_n a)}\right)}{\left[\alpha_n \sinh(\alpha_n L)+\frac{h_\infty}{k}\cosh(\alpha_n L)\right]\frac{a^2}{2}\left(J_1^2(\alpha_n a)\right)+J_0^2(\alpha_n a)} \tag{4}$$

Then the result of the temperature distribution for the rotor-shaft is obtained as:

$$T-T_\infty=\theta=\frac{W_i a^2}{4k}\left(1-\frac{r^2}{a^2}\right)+\frac{W_i a^2}{2h}+\sum_{n=1}^{\infty} C_n \cosh(\alpha_n Z) J_0(\alpha_n r) \tag{5}$$

Since the analytical solution is the summation of an infinite series, only a finite number of terms are considered while obtaining the analytical solution after checking the effect of the number of terms on the result. In other words, the equations are evaluated until the change in the temperature is less than the desired tolerance. And it is found that the solution converges with more than 5 terms, and it does not change appreciably when an additional number of terms is used. The results are obtained in terms of a series expansion solution involving Bessel functions based on the principle of superposition and separation of variables, and comparison between the analytical results and the numerical results obtained through FEA package, ANSYS™ which is stated below. The comparison shows that they are in excellent agreement. The analytical solution is useful, as it can be achieved with basic math solvers and handheld calculators. It can also be used to confirm numerical schemes or compare with experimental data. The representation of these analytical results is given in the following figures.

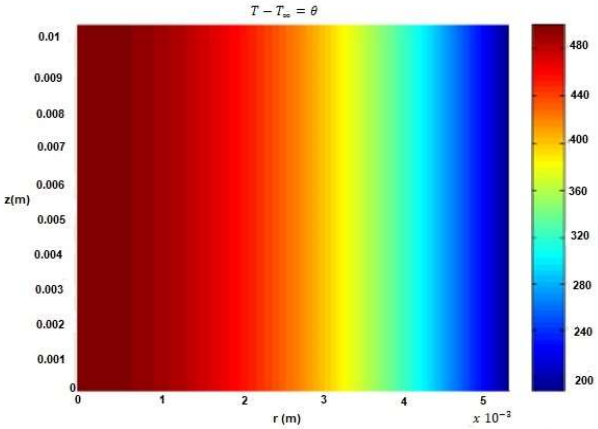

Figure 13. 2D plots of θ in MATLAB.

Firstly, θ is plotted within MATLAB™ as shown in Figure 13 and Figure 14 below, to visualize how their summation together with ambient temperature form the result of the temperature distribution. In Figure 14, the 3D-view of T (r, z) together with its surface-map onto base is a good qualitative overview of the full space temperature distribution for the analytical rotor-shaft model. However, the Analytical solutions of rotating cartesian coordinates can be found in the appendix section, under appendix C.

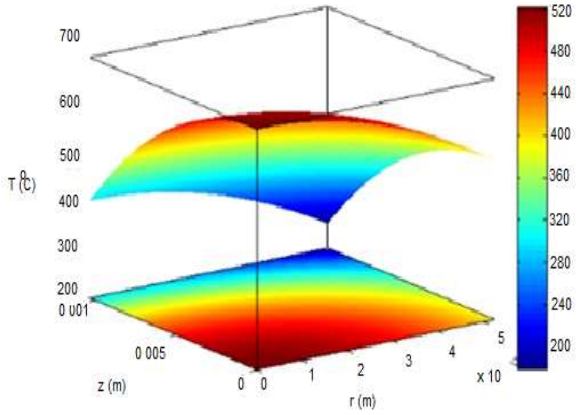

Figure 14. 3D plot in MATLAB of the analytical temperature distribution as a function of distance in r-direction (m) and in z-direction (m) in a rotor-shaft model.

5. Comparison results of the analytical method and the numerical method.

The temperature profiles get closer between these solutions in the r or z directions. The results are obtained in terms of a series of expansion solutions involving Bessel functions based on the principle of superposition and separation of variables and superposition only in three variables. The eigenvalues required by the series expansion are solved by root-solving methods making use of both the orthogonality of the Bessel functions and homogeneous boundary conditions. Figure 15 illustrates temperature variation between analytical and numerical results in the r-direction. Figure 16 illustrates temperature variation between analytical and FEM results in the z-direction.

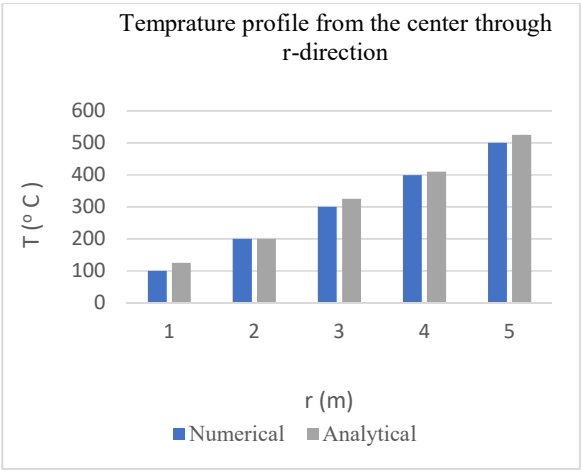

Figure 15. Comparison of temperature variation between analytical and FEM results through r–direction.

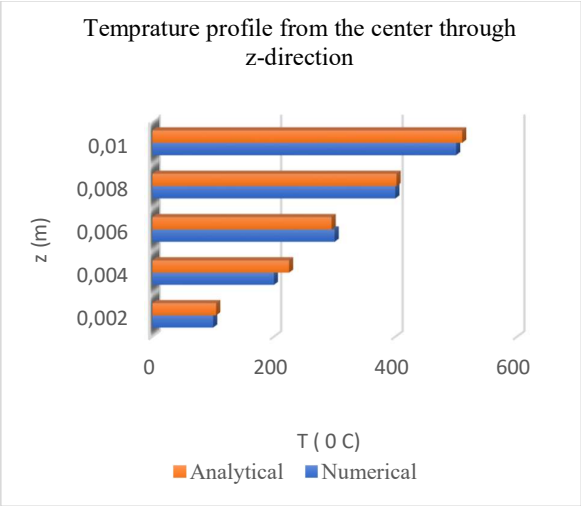

Figure 16. Comparison of temperature variation between analytical and FEM results through z–direction.

6. Conclusion

The analytical solution can be used to obtain an accurate temperature distribution in any location of the object as an alternative to a large population of temperature values in grid points. Also, we present the results by comparing and discussing the analytical modal analysis, and analytical transient thermal analysis. A comparison between numerical and experimental analyses is provided using graph plots, which we discuss in detail. In addition, we draw the following conclusions based on our findings:

- A thermal analytical model is proposed, which validates our numerical simulations, this model allows us to quantify the duration of temperature transient effects.
- The axial location, where the asymmetric temperature distributions occur, matters in evaluating thermal vibrations. It is found that the thermal vibrations are strengthened when significant temperature gradients occur in the cross-sections exhibiting higher vibrations in operation.
- The thermal vibration is influenced by many factors including the shaft size, rotational speeds, heating locations, critical speed, etc. For rotors with different structures, it is not suitable to compare the thermal responses directly due to the dependence of the sensitive operational conditions on the shaft size.
- The higher the thermal convection coefficient H is, the lower the thermal vibration will be induced. And a similar trend was found for the heat conductivity k of rotor material. However, because k influences the thermal vibration from more aspects, the descending ratio of the amplitudes with the increase of k differs from that of H for thermal vibrations.

Nomenclature

APDL	Ansys parametric design language
ANSYS	Analysis system
BCs	Boundary conditions
CAD	Computer-aided design
CAE	Computer-aided engineering
CFD	Computational fluid dynamics
CHT	Conjugate heat transfer
DOF	Degree of freedom
EMA	Experimental modal analysis
FEA	Finite element analysis
FEM	Finite element method
FFT	Fast Fourier transform
FRF	Frequency response function
HP	High pressure
PDEs	Partial differential equations
TGs	Temperature gradients

Acknowledgement

This project is supported by Department of Mechanical Engineering Nnamdi Azikiwe University, Awka Nigeria, and Department of Mechanical and Mechatronics Engineering Tshwane University of Technology Pretoria, South Africa.

Conflicts of Interest

The authors confirm that the publication of this article causes no conflicts of interest.

Data and Materials Accessibility

Supplementary materials and data used in this research are accessible upon request. For access, please contact the corresponding author.

Reference

[1] L. Sátor, V. Sladek, J. SLadek, "Transient analysis of FGM plates bending under thermal loading: comparative study within classical and generalized thermos elasticity," *MATEC Web of Conferences,* vol. 254, 2019, pp. 1-10.

[2] R. R. Vegesna, D. Checcacci, G. Girezzi. "Thermal Bowing of Steam Turbine Shafts: Prediction Methods and Field Data Matching," *Turbo Expo: Power for Land, Sea, and Air,* vol. 85987, American Society of Mechanical Engineers, 2022.

[3] J. Badur, M. Bryk, "Accelerated start-up of the steam turbine by means of controlled cooling steam injection," *Energy,* vol. 173, pp. 1242-1255, 2019.

[4] H. Nomoto, "Solid particle erosion analysis and protection design for steam turbines," in *Advances in steam turbines for modern power plants*, Woodhead Publishing, 2022, pp. 267-286.

[5] M. Geveci, "Fault Tolerant Thermal Control of Steam Turbine Shell Deflections," *arXiv:1703.00079 [cs.SY]*, 2017, https://doi.org/10.48550/arXiv.1703.00079

[6] K. R. Shetkar, J. Srinivas, "Localized damage identification in the last stage low-pressure steam turbine blade using dynamic parameter measurements," *Journal of Nondestructive Evaluation, Diagnostics and Prognostics of Engineering Systems,* vol. 6, no. 1, 2023.

[7] D. Toebben, P. Łuczyński, M. Diefenthal, M. Wirsum, S. Reitschmidt, W. F. D. Mohr, K. Helbig, "Numerical investigation of the heat transfer and flow phenomena in an ip steam turbine in warm-keeping operation with hot air," in *Proceedings of the ASME Turbo Expo 2017: Turbomachinery Technical Conference and Exposition,* vol. 8, Charlotte, North Carolina, USA. June 26–30, 2017.

[8] B. Lübbe, J. Aschenbruck, O. Pütz, M. Theidel, "Design and Validation of a Large Steam Turbine End-Stage Blade to Meet Current and Future Market Demands," in *Proceedings of the ASME Turbo Expo 2021: Turbomachinery Technical Conference and Exposition,* vol. 8, Virtual, Online. June 7–11, 2021.

[9] M. Teixeira Júnior, G. Zilio, M. V. V. Mortean, K. V. de Paiva, J. L. G. Oliveira, "Experimental and numerical analysis of transient thermal stresses on thick-walled cylinder", *International Journal of Pressure Vessels and Piping*, vol. 202, 104884, pp. 1-12, 2023.

[10] S. Chatterton, P. Pennacchi, A. Vania, "On the Effects of a Shaft Crack Propagation on the Dynamic Behavior of a Steam Turbine," in *Proceedings of the ASME Turbo Expo 2020: Turbomachinery Technical Conference and Exposition. Volume 10B: Structures and Dynamics*, Virtual, Online, September 21–25, 2020.

[11] T. Diurno, T. Fondelli, L. Nettis, N. Maceli, L. Arcangeli, A. Andreini, Bruno Facchini, "Numerical investigation on the aerodynamic performance of a low-pressure steam turbine exhaust hood using design of experiment analysis," *Journal of Engineering for Gas Turbines and Power,* vol. 142, no. 11, 111006, 2020.

[12] K. D. Rajendra, R. Arakerimath, "Analysis of Steam Turbine Blade Failure Causes," in *ICRRM 2019–System Reliability, Quality Control, Safety, Maintenance and Management: Applications to Civil, Mechanical and Chemical Engineering*, 2020, pp. 46-52.

[13] A., Bouberle, J. Jakl, J. Liška, "Rotor thermal stress monitoring in steam turbines," *Journal of Physics: Conference Series. 659 012044*, 2015.

Appendix A

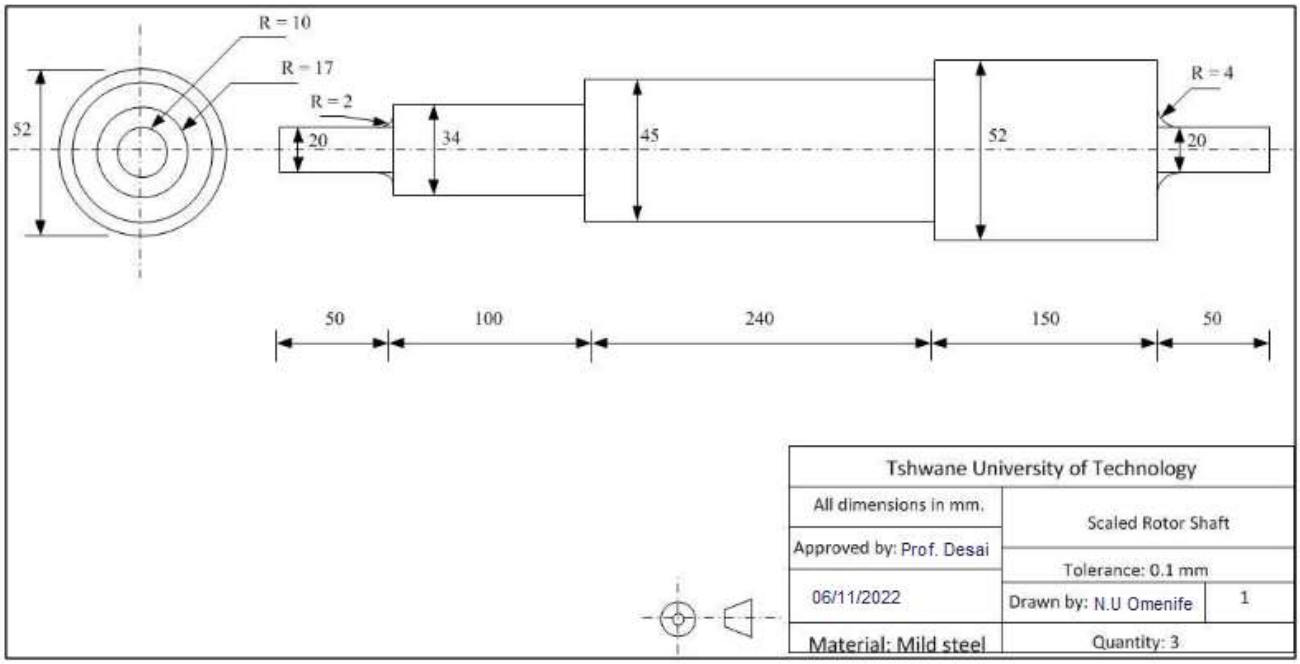
R = 10
R = 17
R = 2
R = 4
52
20
34
45
52
20
50
100
240
150
50
Tshwane University of Technology
All dimensions in mm.
Scaled Rotor Shaft
Approved by: Prof. Desai
Tolerance: 0.1 mm
06/11/2022
Drawn by: N.U Omenife
1
Material: Mild steel
Quantity: 3

Appendix B

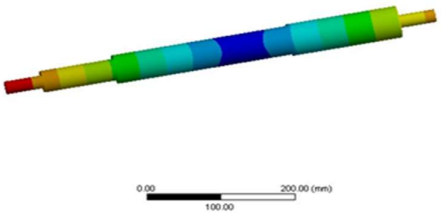

Mode 0

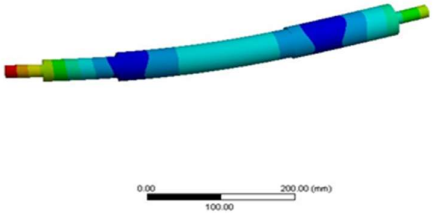

Mode 1

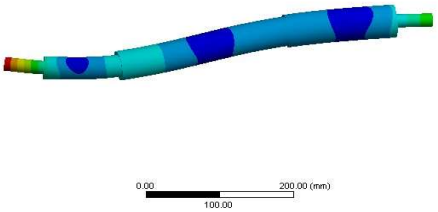

Mode 2

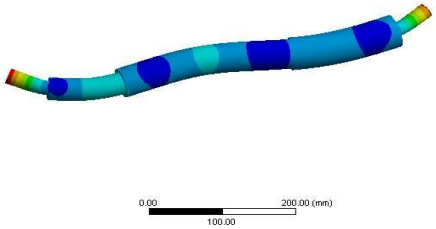

Mode 3

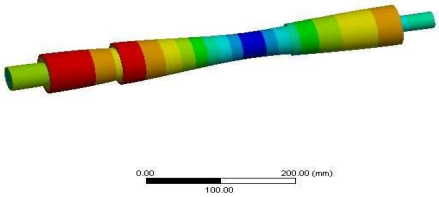

Mode 4

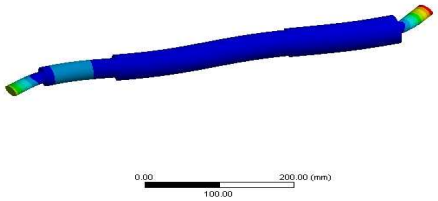

Mode 5

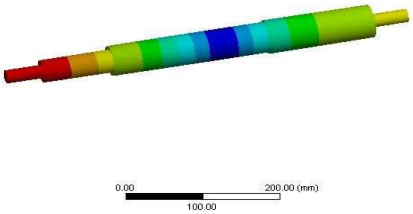

Mode 6

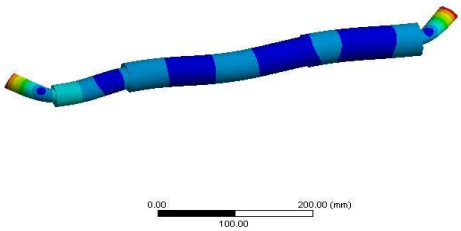

Mode 7

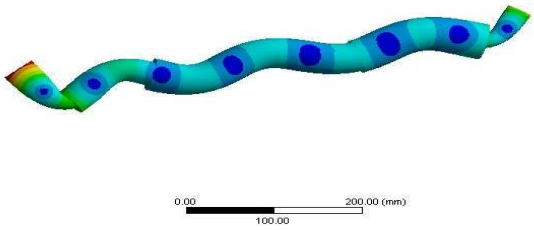

Mode 9

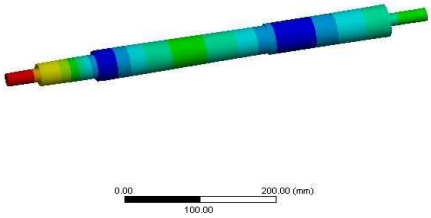

Mode 10

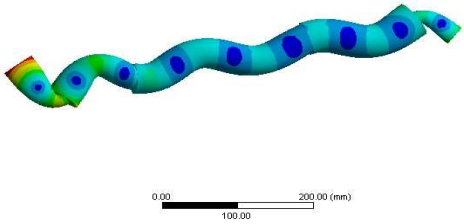

Mode 11

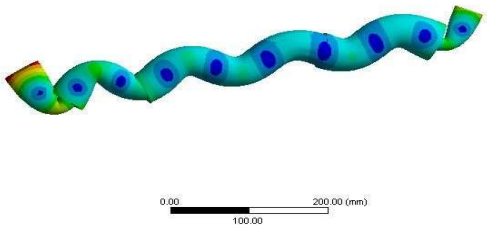

Mode 12

Appendix C

In the rotating Cartesian coordinates, the strain resulted from the thermal expansion is thus obtained as,

$$\varepsilon_{xT}(\xi,n,z,t)=\varepsilon_{yT}(\xi,n,z,t)=\varepsilon_{zT}(\xi,n,z,t)=\alpha.\Delta T(\xi,n,z,t)$$

(Eq. A1)

where α is the linear thermal expansion coefficient. With the existence of thermal strain, the axial stress due to the elastic strain only is expressed as Eq. (A.2)

$$\sigma_z(\xi,n,z,t)=E\left(\varepsilon_z(\xi,n,z,t)-\frac{1}{1-2v}\varepsilon_{zT}(\xi,n,z,t)\right)$$

(Eq. A2)

where υ is the Poisson ratio and εz is the total strain. The components of εz due to the deformations in ξ and η directions equal to

$$\varepsilon_{z\xi}(\xi,n,z,t)=-\xi(\xi,n,z,t)\frac{d^2x_\xi(z,t)}{dz^2}$$

$$\varepsilon_{zn}(\xi,n,z,t)=-n(\xi,n,z,t)\ \frac{d^2y_n(z,t)}{dz^2}$$

(Eq. A3)

where xξ(z,t) is the deformations along axis ξ and yη(z,t) along axis η. Furthermore, the axial thermal stress according to the thermal strain is:

$$\sigma_{zT}(\xi,n,z,t)=\frac{E}{1-2v}\varepsilon_{zT}(\xi,n,z,t)=\frac{E\alpha}{1-2v}\Delta T(\xi,n,z,t)$$

(Eq. A4)

As a result, the axial stress components due to xξ(z,t) and yη(z, t) is ultimately obtained as Eq. (A.5) by substituting Eq. (A.3) into Eq. (A.2).

$$\left.\begin{aligned}\sigma_{z\xi}(\xi,n,z,t)&=-E.\xi(\xi,n,z,t)\frac{d^2x_\xi(z,t)}{dz^2}-\sigma_{zT}\\ \sigma_{zn}(\xi,n,z,t)&=-E.n(\xi,n,z,t)\ \frac{d^2y_n(z,t)}{dz^2}-\sigma_{zT}\end{aligned}\right\}$$

(Eq. A5)

During the vibration, the stress-related bending moments about axis of ξ and η equal to the integral of Eq. (A.5) over the cross-section area, as follows:

$$\left.\begin{aligned}M_\xi(z,t)&=\int_A zn(\xi,n,z,t)n(\xi,n,z,t)d\xi dn\\&=-EI_\xi\frac{d^2y_n(z,t)}{dz^2}-M_{T\xi}(z,t)\\ M_n(z,t)&=\int_A z\xi(\xi,n,z,t)\xi(\xi,n,z,t)d\xi dn\\&=-EI_n\frac{d^2y_n(z,t)}{dz^2}-M_{Tn}(z,t)\end{aligned}\right\}$$

(Eq. A6)

where MTξ(z,t) and MTη(z,t) are the equivalent thermal moment components with respect to the axis ξ and η as shown in Eq. (A.6). Because the temperature is solved in the cylindrical coordinates, for simplicity of analysis, the calculation of thermal moments here should be performed in the same coordinate system as well, there follows:

$$\left.\begin{aligned}M_{T\xi}(t-t_{nr})I_z=z_0&=\int A^\sigma zT(r,\theta,z,t)r^2\,sin\theta\ dr\ d\theta\\ M_{Tn}(t-t_{nr})I_z=z_0&=\int A^\sigma zT(r,\theta,z,t)r^2\,cos\theta\ dr\ d\theta\end{aligned}\right\}$$

(Eq. A7)

It should be noted that a constant thermal stress, which exists only in the even temperature for an isotropic material, will lead to zero thermal moments, as implied by Eq. (A.7). It should be noted that a constant thermal stress, which exists only in the even temperature for an isotropic material, will lead to zero thermal moments, as implied by Eq. (A.7). This fact demonstrates the reliability of the equivalent-thermal-moment model in investigating how TGs influence the rotor vibrations. By derivation of the moments with respect to the axial coordinate, the shearing force components are finally expressed as functions of the deformations and equivalent thermal moments, shown as:

$$\left.\begin{aligned}P_\xi&=\frac{dM_n}{dz}=-EI_n\frac{d^3X_\xi}{dz^3}-\frac{dM_{Tn}}{dz}\\ P_n&=\frac{dM_\xi}{dz}=-EI_\xi\frac{d^3Y_n}{dz^3}-\frac{dM_{T\xi}}{dz}\end{aligned}\right\}$$

(Eq. A8)